CrossMark

ORIGINAL PAPER

Analysis of Gateroad Stability in Relation to Yield Pillar Size: A Case Study

Guang-chao Zhang[1] · Fu-lian He[1] · Hong-guo Jia[2] · Yong-hui Lai[1]

Abstract This paper presents an integrated approach for field test and numerical modelling to investigate the relationship between gateroad stability and yield pillar size. The test site is located at Yuncheng city, Shanxi Province, China. Field tests indicated that when the yield pillar width was 17 m, the total convergence of the roof, yield pillar rib and virgin coal rib were 882, 587 and 352 mm, respectively, and severe roof sagging and yield rib spalling occurred during the panel retreat. A meticulously validated numerical model, incorporating a double-yield model for the gob materials and calibrated parameters, was developed to investigate the stress changes and yield zone distribution across the yield pillar with different sizes. The results of the simulation indicate that a yield pillar 17 m wide puts the gateroad in a high-stress environment; conversely, a yield pillar 8 m wide is subjected to a relatively low load and puts the gateroad in a good stress environment. Consequently, the rational yield pillar width was estimated at 8 m, and a support strategy was proposed. Field measurement data demonstrate that the newly designed pillar size and support pattern can efficiently ensure gateroad stability. The proposed numerical simulation procedure and calibrated method could be a viable alternative approach to yield pillar design. In addition, the design principle and support strategy for the yield pillar presented in this study can potentially be applied to other similar projects.

✉ Guang-chao Zhang
  zgchao2015@163.com

1 College of Resources and Safety Engineering, China University of Mining and Technology (Beijing), Beijing 100083, China

2 College of Mining and Safety Engineering, Shan Dong University of Science and Technology, Qingdao 266510, China

1 Introduction

The stability of gateroads is essential for the safe and effective operation of the longwall panel (Cheng et al. 2010). The yield pillars formed in the adjacent longwall panels are mainly employed to protect the gateroads of current panels from the effects of excessive closure (Whittaker and Singh 1981). However, an unsuitable yield pillar design could lead to frequent roof falling, rib spalling and support body failure, due to mining-induced high stress, thus resulting in serious instability of the rock mass around the gateroad. The design of the yield pillar is therefore important for ensuring a safe and stable gateroad condition and long-term mine safety and productivity. To date, many attempts have been made to obtain a comprehensive understanding of a rational yield pillar design, and many empirical, analytical and numerical methods have been developed.

Based on the database regarding yield pillars in South African coal mines, Salamon and Munro (1967), Salamon (1970), and Salamon et al. (1998) proposed an empirical formula which correlated the pillar strength with pillar width-to-height ratio, which has been widely applied to pillar designs worldwide. At the same time, Galvin et al. (1999) investigated and analysed a large number of pillars in Australian coal mines and developed a similar strength formula. Based on the field data collected in the UK coal mines, Whittaker and Singh (1981) investigated the relationship between gateroad stability and yield pillars with different sizes. Medhurst and Brown (1998) presented the relationship between the strength of coal mass, pillar

🗔 Springer

width-to-height ratio and pillar strength. Their study was performed by testing the strength of coal sample with different sizes via a set of triaxial compression tests. In 1974, Wagner (1974) investigated the complete stress–strain relationship of yield pillars with different shapes in a coal mine, and revealed that an intact core zone in pillars plays an important role in its stability. Sheorey et al. (1982) presented analytical formulae for pillar design by analysing the abutment pressure across the pillar and concluded that gateroads located in high-stress environments may be subjected to coal bumps. However, their model neglected the influence of gateroads excavation on abutment pressure distribution. Based on the field data obtained from American coal mines, Esterhuizen et al. (2011) developed an equation to estimate the pillar strength, taking into account the intact rock strength and the potential impact of large angular discontinuities on pillar strength. In 2014, Gao (2014) developed an equation to estimate the width of non-elastic zone in an inclined coal pillar, which takes into account the plastic softening nature of coal and the coal seam pitch. Based on estimated subsidence, Chen et al. (2016) developed a strip coal pillar design approach and successfully applied to Daizhuang Coal Mine in China. Yu et al. (2016) investigated the stress changes and deformation of a longwall pillar in Tashan coalmine, China, using an integrated stress and displacement monitoring system.

In reality, the strength of yield pillars is closely associated with factors such as its size and shape, the mechanical properties of surrounding rock strata, the state of in situ stresses, the mining sequence and the nature of bedding planes. Although the empirical and analytical methods mentioned above have been widely used in the yield pillars design, their applications are limited because they cannot include various factors in their methods. However, as numerical modelling is an effective method of incorporating various factors in the analysis, the results may be more realistic than those obtained by previous analytical and empirical approaches. In recent years, an increasing number of numerical modelling studies have been developed on yield pillar designs. Based on a case study conducted at Zhaogu No.2 mine, China, Jiang et al. (2016) developed a tension-weakening model for gateroad stability analysis, considering the weakening effect of fractures on the stiffness of the rock mass. Wang et al. (2016) proposed an approach for simulating static and dynamic behaviour of coal pillars using FLAC3D software and investigated the failure mechanisms and dynamic response of a coal pillar. However, after reviewing some of previous studies, we found two major limitations in their modelling simulations: (1) because yield pillars are subjected to a complex loading–unloading pattern during their service life, the relevant modelling technology is still a work in progress, and a more rigorous modelling procedure

and parameter-calibrated approach is required to provide more realistic results; and (2) the gob compaction process must be considered in the yield pillar design, since it can cause stress changes in the two ribs by providing an additional support resistance to the roof strata; nevertheless, existing studies have rarely taken these limitations into account. Cheng et al. (2010) built a three-dimensional simulation model using FLAC3D code for the design of coal pillars in an inclined thick coal seam. In their model, the gob is filled with elastic materials with a Young's modulus of 190 MPa and a Poisson's ratio of 0.25; however, no viable validation was performed on the input parameters. Li et al. (2014, 2015) developed a numerical model using FLAC3D code to investigate two cases of yield pillar application in Chinese mines, in which double-yield models were adopted to simulate gob materials. In light of these limitations, a meticulously validated numerical model, incorporating a double-yield model for the gob materials and calibrated parameters, was developed in the current study to analyse the stability of yield pillars in underground coal mines.

This paper investigates the gateroad stability in relation to yield pillar size based on a field test, case studies and numerical modelling for back analysis. The arrangement is listed as follows. In Sect. 2, the geological and mining conditions, as well as the in situ measurements showing the failed yield pillar design, were first presented. In Sect. 3, a numerical model, incorporating a double-yield model for gob materials and calibrated parameters, was then developed and validated against the in situ measurement data. In Sect. 4, the stress changes and yield zones distribution across the yield pillar with six different sizes were numerically investigated in detail, thus allowing the determination of a reasonable yield pillar width and support strategy; its reliability was verified by performing field applications in Sect. 5. The proposed numerical simulation procedure and calibrated method, overcoming the limitations mentioned above, may perhaps be considered as a viable alternative approach to yield pillar design. In addition, the design principle and support strategy for yield pillar presented in this study can potentially be applied in other similar projects.

2 Case Study

2.1 Mining and Geological Condition

This case study focuses on a coal mine located in Yuncheng city, Shanxi Province, China (Fig. 1). The current mining seam is #2 coal seam. The average overburden depth and thickness of the coal seam are 298 and 6.3 m, respectively. The rock strata above the coal seam are, in
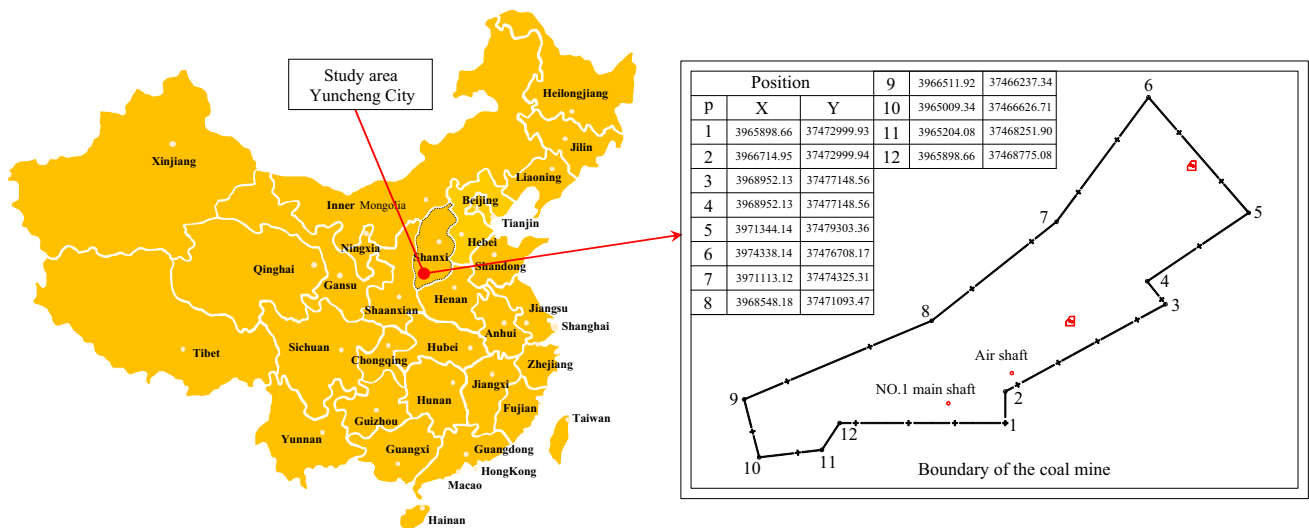
Fig. 1 Location of the test site

order, sandy mudstone (2.9 m), siltstone (12.4 m) and mudstone (3.2 m), while the rock strata below the coal seam are, in order, mudstone (1.6 m), siltstone (6.1 m) and fine sandstone (9.2 m). Figure 2 shows the generalised stratigraphy column.

This study involves mining panels N2101, N2102 and N2103, which are each approximately 260 m in strike and 1400 m in dip. A fully mechanised longwall top-coal caving method is used for #2 coal extraction, with a mechanised mining height of 3.5 m. N2102 panel is located at the centre of mining area No. 2. N2101 panel, where the coal has been extracted, is located north of N2102 panel, and N2103 panel, which is under development, is located south of N2103 panel, as illustrated in Fig. 3. The yield pillar between N2101 tailgate and N2102 headgate is 17 m wide by 3.5 m high.
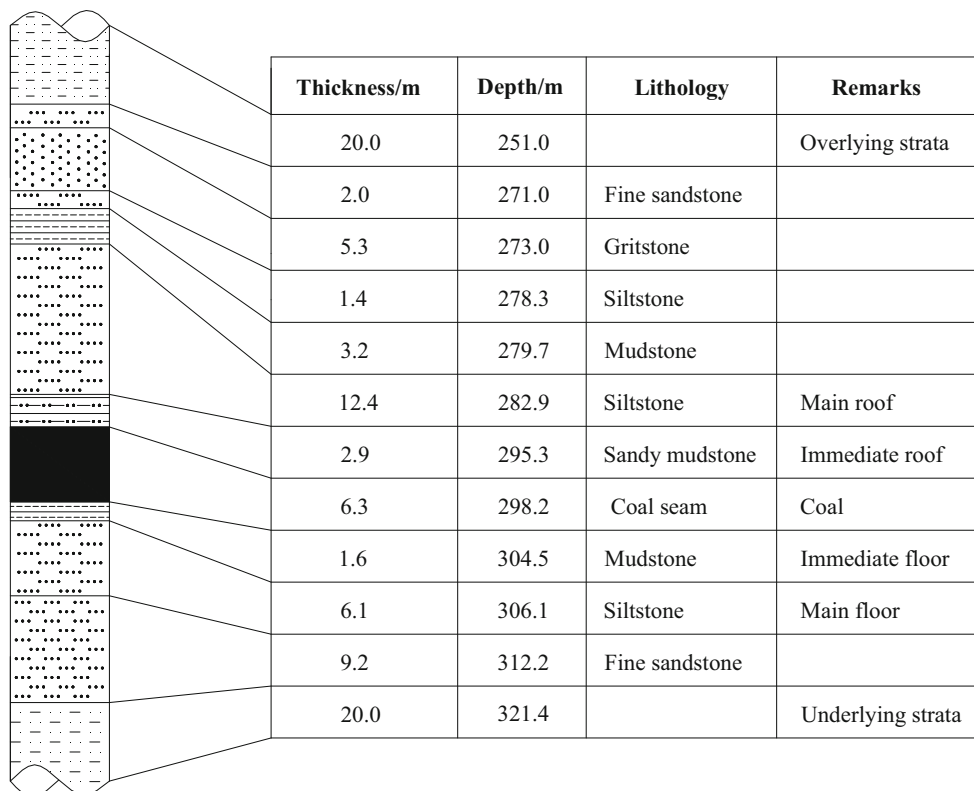

Thickness/m	Depth/m	Lithology	Remarks
20.0	251.0		Overlying strata
2.0	271.0	Fine sandstone	
5.3	273.0	Gritstone	
1.4	278.3	Siltstone	
3.2	279.7	Mudstone	
12.4	282.9	Siltstone	Main roof
2.9	295.3	Sandy mudstone	Immediate roof
6.3	298.2	Coal seam	Coal
1.6	304.5	Mudstone	Immediate floor
6.1	306.1	Siltstone	Main floor
9.2	312.2	Fine sandstone	
20.0	321.4		Underlying strata

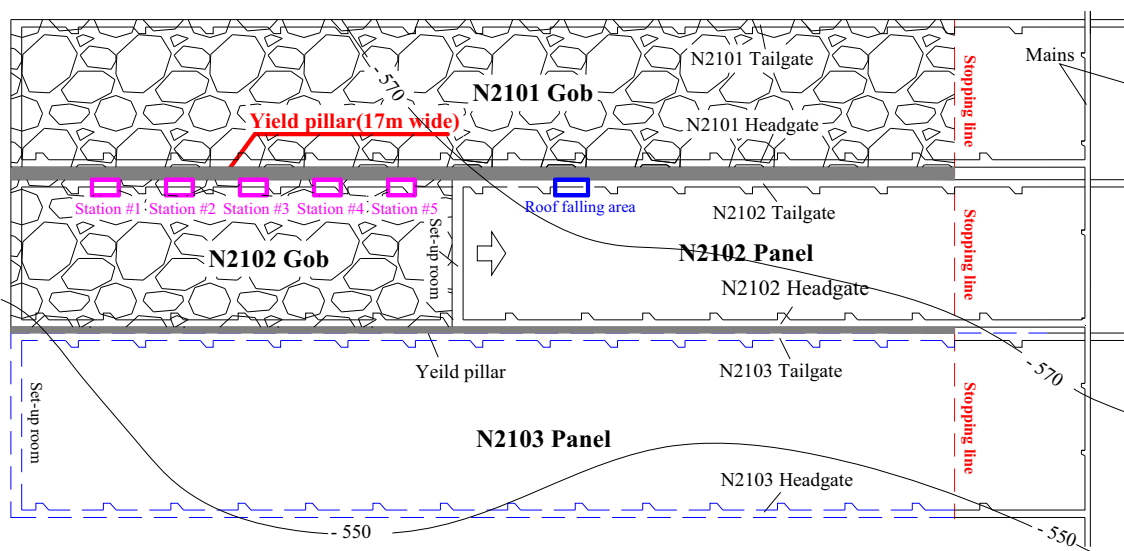**Fig. 2** Generalised stratigraphy column of the test site

Fig. 3 Layout of N2101, N2102 and N2103 panels

All gateroads have a rectangular cross section supported by bolt-mesh-cable. The section is 5 m wide and 3.5 m high.

The bolts 20 mm in diameter and 2500 mm in length were used for the roof support, and the bolts 18 mm in diameter and 2000 mm in length were used to support the two ribs. All bolts were installed with a spacing of 900 mm × 1000 mm. The roof was secondarily supported by anchor cables 17.8 mm in diameter and 6300 mm in length. The anchor cables were installed with a spacing of 2000 mm × 2000 mm. All bolts were set up in combination with steel mesh and steel ladder beams. The two anchor cables of each row were installed on the channel beams. Figure 4 presents a cross section of the bolt and cable support.

2.2 Rock Mechanical Properties Experiments

To better understand the mechanical properties of the rock mass surrounding the entry, laboratory tests were carried out on the coal and rock samples collected from the N2102 tailgate. The tests were conducted on a servo-controlled testing system (TAW-2000), having a maximum axial load of 2000 kN, a maximum shear load of 500 kN and a maximum lateral pressure of 500 kN. The uniaxial compressive strength, Young's modulus and Poisson's ratio were obtained by conducting uniaxial compression tests, while the cohesion and friction angle were estimated by conducting triaxial compression tests. For each specific geological unit, three specimens were tested. Based on the results of these tests, the mechanical parameters of each geological unit are shown in Table 1. The coal seam was found to be weak coal with a uniaxial compressive strength

of 13.7 MPa, and the gateroad was generally excavated in the coal seam; thus, it can be predicted that the weak properties of coal contribute significantly to the deformation of a gateroad once it is excavated.

2.3 In Situ Measurement

To evaluate the feasibility of the current pillar size, the deformation of the rock masses surrounding the N2102 tailgate during the gateroad development and panel retreat period was recorded. Five measurement stations were arranged immediately after the N2102 tailgate development. The interval between each station was 100 m. Figure 3 shows the location of these stations. The following describes the details of the measurements, including the apparatus, its in situ installation and the data collection:

1. For each measurement station, permanent pegs (blue solid circles in Fig. 5a) were installed in the roof, floor, yield pillar rib and virgin coal rib, respectively. Among them, the roof and floor pegs were installed at the mid-span of the roof and floor, while two rib pegs were installed 1.7 m away from the floor.
2. During the observation, the two ribs convergences were measured using a flexible tape and measuring lines, while the roof and floor convergences were measured using telescopic measuring rods and measuring lines (see Fig. 5b).
3. In the field, the data were collected by specialist technicians in the manual metre reading method once every 2 days. Measurements lasted throughout the development of the N2102 tailgate until the N2102 panel passed the station.

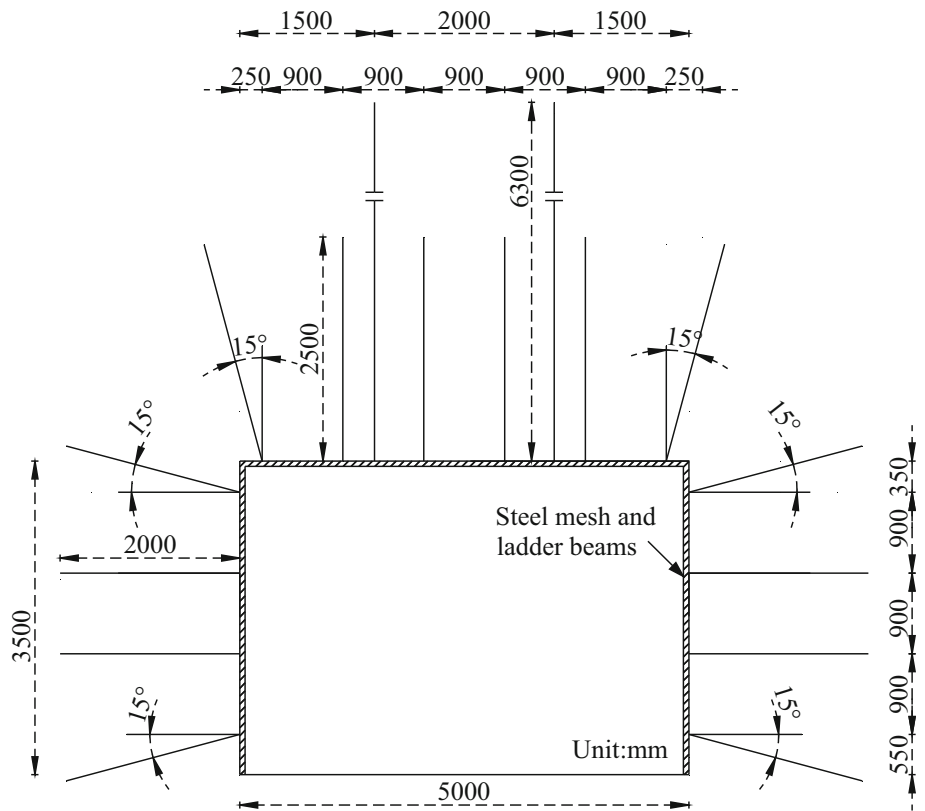**Fig. 4** Gateroad section
supported by bolt-mesh-cable

Table 1 Mechanical properties of each geological unit

Lithology	E_i (GPa)	σ_c (MPa)	σ_t (MPa)	υ	C (MPa)	Φ (deg)
Gritstone	56.8	53.2	2.52	0.22	12.5	32
Siltstone	53.5	43.7	2.15	0.24	11.3	30
Sandy mudstone	34.5	32.2	2.36	0.27	8.7	28
Coal	7.2	13.7	1.27	0.32	3.4	24
Mudstone	12.5	26.1	1.85	0.30	7.3	26
Fine sandstone	65.5	58.6	3.25	0.24	15.4	34

E_i is modulus of elasticity, σ_c is uniaxial compressive strength, σ_t is tensile strength, υ is Poisson's ratio, C is cohesion, ϕ is the friction angle

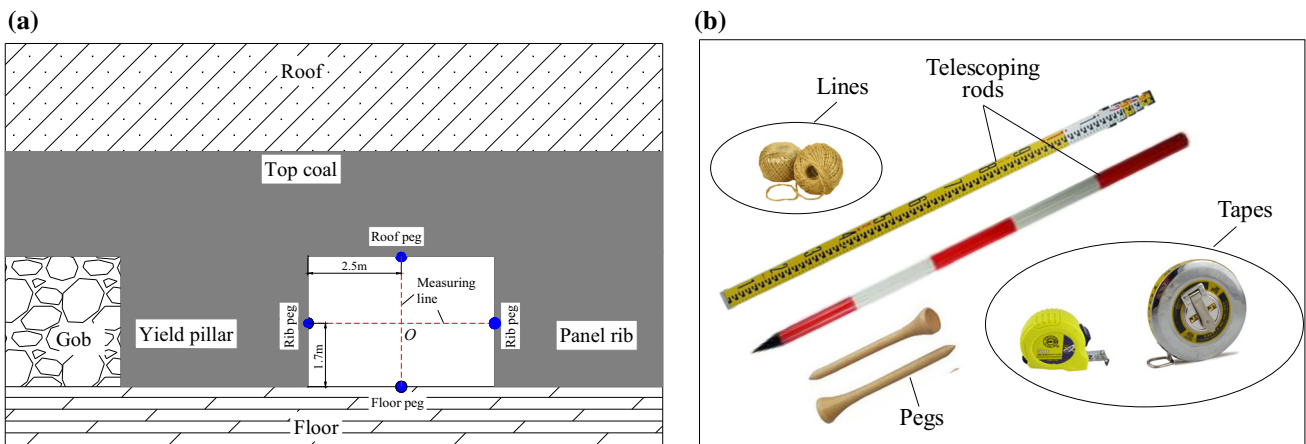**Fig. 5** Schematic diagram for entry convergence measurement **a** cross section of the measurement station, **b** measurement apparatus
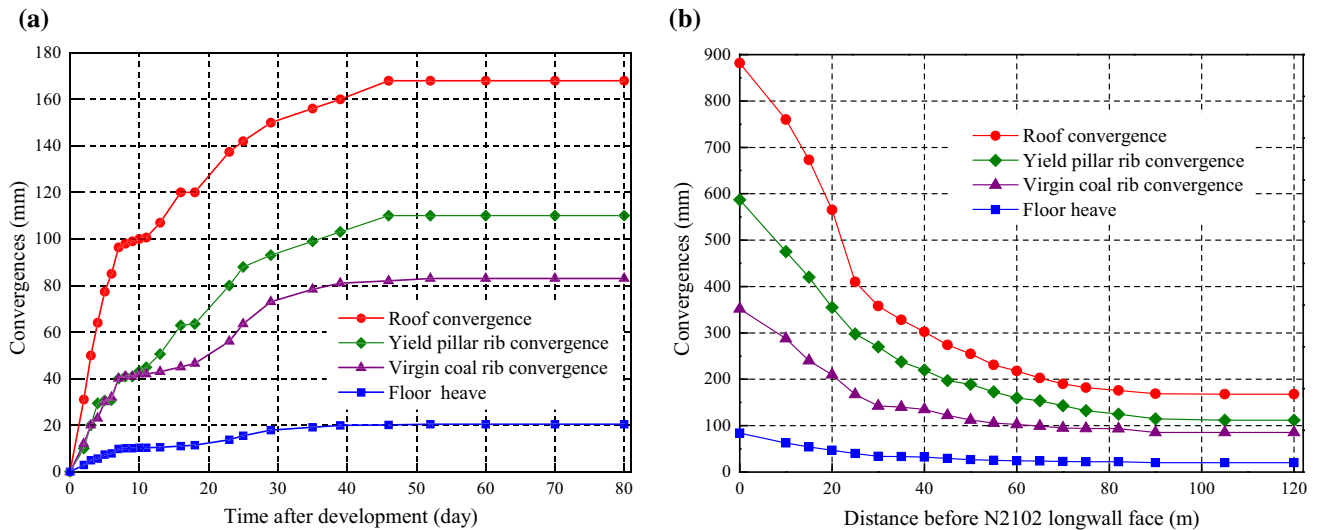
(a)

(b)

Fig. 6 Measured convergences in N2102 tailgate **a** during N2102 tailgate development period, **b** during N2102 panel retreat period

Because the results in each measurement station have almost the same tendencies, only the measurement data from the station #3 are used for the analysis. Figure 6 shows the results of the N2102 tailgate convergence at different stages. As shown in Fig. 6a, the gateroad deformation mainly built up within 40 days after N2012 development, and then, the deformation rate became almost zero. The total convergence of the roof, yield pillar rib and virgin coal rib reached 168, 110 and 83 mm, respectively. During the N2012 panel retreat period, the gateroad deformation increased considerably compared to that in the development period (see Fig. 6b), and more than 90% of the gateroad convergence took place after the longwall face advanced approximately 30 m towards the measurement station. The total convergence of the roof, yield pillar rib and virgin coal rib increased to 882, 587 and 352 mm, respectively. These results clearly indicated that maximum deformation arose at the roof strata and the yield pillar deformation was secondary; floor heave was remarkably smaller than the roof sag and rib convergence. This can be attributed to the geological properties of the surrounding rock. Because the gateroad was excavated along the floor line of the coal seam, the immediate roof and two ribs were composed of weak coal, while the floor was composed of relatively stronger mudstone and siltstone. The poor mechanical properties of the coal mass directly induced the large deformation of the roof and two ribs.

The field observations also found that severe roof sagging and yield rib spalling occurred frequently during the N2102 panel retreat (Fig. 7a, b). It should be noted that a severe roof-falling accident occurred about 20–30 m before the working face (blue rectangle in Fig. 3), which is about 610 m away from the stopping line, as shown in Fig. 7c. It

took about 2 weeks to rehabilitate the failed entry, resulting in a considerable amount of extra labour, financial resources and time loss. No evidence of unfavourable geological conditions remains in the roof-falling area. This large deformation of the roof and yield pillar might be attributed to the low coal strength and high stress induced by the panel retreat. Therefore, more attention should be paid to the roof and yield pillar support during the panel retreat period.

These in situ measurements indicate that the current pillar size and support pattern are ineffective for gateroad stability, and the loss of coal reserve was serious. Hence, to mitigate gateroad deformation in the following panels, a more rational yield pillar size and support design needs to be considered.

3 Numerical Model Generation

3.1 Numerical Simulation Model and Simulation Plans

A numerical model using FLAC3D software was developed to investigate the relationship between gateroad stability and pillar sizes. The dimensions of the model were 270 m × 90.4 m × 1 m, which were determined based on model sensitivity analysis with regard to size and mesh density. One half of each of the N2101 and N2102 panels and the gateroads system were incorporated in the model, as shown in Fig. 8. A vertical stress of 7.5 MPa was applied at the top model boundary to simulate an overburden pressure by assuming the overlying unit weight is 0.025 MN/m^3, and gravity force was applied. The horizontal displacements of the four vertical planes of the
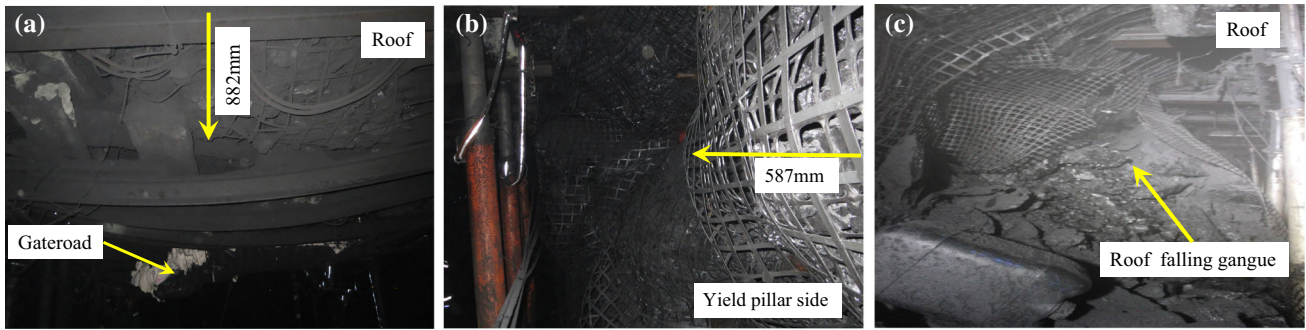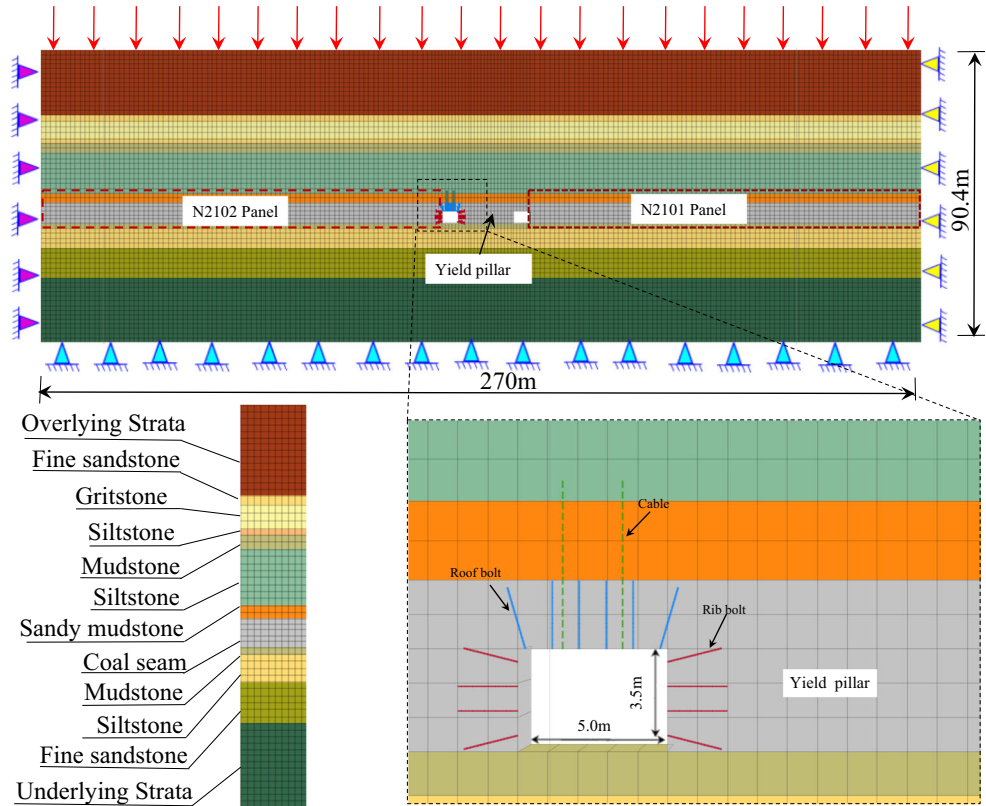
Fig. 7 Conditions of N2102 tailgate during the panel retreat period. **a** Roof sag, **b** yield pillar spalling, **c** Roof falling

Fig. 8 Configuration of the model performed using FLAC3D and bolts/cables support pattern

model were restricted in the normal direction, and the vertical displacement at the base of the model was set to zero. Based on a study carried out at a nearby mine (Zhang and He 2016), in situ stresses were applied in the form of initial stress with the horizontal-to-vertical stress ratio set to 1.2 in the x- and y-directions. The Mohr–Coulomb model was used for the rock strata modelling, the strain-softening Mohr–Coulomb model was used for the yield pillar and the double-yield model was used for the gob modelling; these are defined in later Sects. 3.2 and 3.3.

Considering the effect of the support on rock mass response, a gateroad with a rectangular cross section 5 m wide and 3.5 m high was simulated in the model. The

bolts/cables support presented in Fig. 4 were simulated by the cable structure element embedded in FLAC3D. Table 2 lists the mechanical and geometric parameters of the cable structure element.

In this simulation, the numerical model was solved using the following steps: (1) the calculation of the initial stress caused by gravity, (2) the development of the N2101 headgate, (3) the retreat of the N2101 panel and (4) the development of the N2102 tailgate using six different pillar sizes. Based on the mining condition of N2102 panel, the height of the yield pillar is set to 3.5 m, and the yield pillar widths are simulated in the model, i.e. 20, 17, 14, 11, 8 and 5 m.

Table 2 Mechanical and geometric parameters of cable structure element (Zhang et al. 2014)

Type	E (GPa)	C_g (N/m)	K_g (N/m^2)	ρ_g (m)	A (m^2)	F_t (N)
Roof bolt	200	4.7e5	5.6e9	8.79e−2	3.14e−4	1.6e5
Ribs bolt	200	4.7e5	4.3e9	8.79e−2	2.54e−4	1.3e5
Cable	195	4.7e5	4.2e9	8.79e−2	2.49e−4	2.5e5

E is the Young's modulus, C_g is the grout cohesive strength per unit length, K_g is the grout stiffness per unit length, ρ_g is the grout exposed perimeter, A is the cross-sectional area, F_t is the tensile yield strength

Table 3 Rock strata properties used in the numerical model

Rock strata	Density (kg/m^3)	Bulk modulus (GPa)	Shear modulus (GPa)	Friction angle (°)	Cohesion (MPa)	Tensile strength (MPa)
Overlying strata	2500	8.21	6.02	30	2.0	0.70
Fine sandstone	2800	8.12	5.33	34	3.0	0.65
Gritstone	2720	7.35	5.45	32	2.5	0.50
Siltstone	2750	6.47	4.34	30	2.2	0.43
Mudstone	1800	3.47	2.33	26	1.6	0.37
Siltstone	2750	6.47	4.34	30	2.2	0.43
Sandy mudstone	2320	4.34	2.81	28	1.8	0.50
Coal seam	1412	1.04	0.56	24	0.8	0.25
Mudstone	1800	1.47	1.03	26	1.6	0.37
Siltstone	2750	6.47	4.34	30	2.2	0.43
Fine sandstone	2800	8.12	5.33	34	3.0	0.65
Underlying strata	2500	8.21	6.02	30	2.0	0.70

3.2 Material Properties and Strain-Softening Model for Yield Pillar

A reliable estimation of the mechanical properties of the rock masses was essential for obtaining an acceptable result from the numerical study. Mohammad et al. (1997) suggested that numerical model stiffness is on average 0.469 of the laboratory stiffness and model uniaxial compressive strength is on average 0.284 of the laboratory strength. Cai et al. (2013) suggested that the elastic modulus, cohesion and tensile of coal and rock masses can be estimated at 0.1–0.25 of the laboratory testing results and the Poisson's ratio can be assumed to be 1.2–1.4 of the laboratory testing results. Therefore, the mechanical properties of the coal and rock masses used in the model have been estimated that the elastic modulus, cohesion and tensile strength is 0.2 of the laboratory testing results and the Poisson's ratio is 1.2 of the laboratory testing results. Based on the laboratory testing results (see Table 1), the mechanical properties applied in the model are listed in Table 3.

The deformation and failure of the coal pillars is a complicated and progressive process, which can be divided into the elastic phase, the plastic softening phase and the residual phase. After the coal pillars yield, plastic softening occurs until a residual strength level is achieved (Jaiswal and

Table 4 Variation of mechanical properties of coal with plastic shear strain (Shen 2013)

Plastic strain	0	0.0025	0.005	0.0075	0.01
Cohesion (MPa)	0.8	0.68	0.54	0.40	0.28
Friction angle (°)	24	23	22	21	21

Shrivastva 2009). Currently, the Mohr–Coulomb strain-softening model is the most widely accepted model for the coal pillars, in which the coal pillar is modelled as a nonlinear strain-softening material with cohesion and friction angle softening as a function of plastic strain. Because it is generally difficult to estimate the post-peak properties of a strain-softening model, the strain-softening parameters in this study were estimated based on past experiences in simulating coal and rocks (Shen 2013). Table 4 presents the variation of the cohesion and friction angles with plastic strain.

3.3 Double-Yield Model for Gob Model

3.3.1 Approach for Gob Modelling Based on Double-Yield Model

In longwall mining, when the working face advances far enough, the roof strata behind the face will collapse. The

caved materials are then compacted and consolidated to make it stiffer and to increase its modulus significantly (Yavuz 2004). Investigations have shown that densely compacted gob materials can mitigate the stress concentration in yield pillars because a portion of the vertical load will be undertaken by the consolidated materials (Shabanimashcool and Li 2013). Therefore, the compaction process of gob materials has to be considered during yield pillar design.

In this study, the double-yield model available in FLAC3D is employed to model the strain stiffing behaviour of the gob materials, in which support capacity increases as its volume is gradually compressed induced by roof strata subsidence (Trueman 1990). According to the available literature (Itasca 2007), the cap pressure and materials properties are needed for the double-yield model. The cap pressure parameters can be estimated using Salamon's equation (Salamon 1990), which is given by

$$\sigma = \frac{E_0 \varepsilon}{1 - (\varepsilon/\varepsilon_{max})} \tag{1}$$

where σ is the stress applied to the gob materials, ε is the volumetric strain under the applied stress, ε_m and E_0 are the maximum volumetric strain and initial tangential modulus of the gob materials, respectively. These can be determined by the bulking factor and in situ stress (Yavuz 2004):

$$\varepsilon_{max} = \frac{b - 1}{b} \tag{2}$$

$$E_0 = \frac{1.039 \sigma_c^{1.042}}{b^{7.7}} \tag{3}$$

where σ_c is the compressive strength of the rock pieces, and b is the bulking factor, which can be determined as follows (Peng 2006):

$$b = \frac{h_c + h_{cr}}{h_c} \tag{4}$$

where h_c is the mining height, and h_{cr} is the height of the caved zone.

Investigations have shown that the height of the caved zone, which is closely related to the geological conditions, is about 2–8 times the mining height (Peng 2006). For the N2101 panel, the mining height is 6.3 m, while the height of caved zone is assumed to 26.8 m. Based on the above equation, the bulking factor, maximum strain and the initial modulus of the gob materials can be estimated as 1.235, 0.19 and 16.68 MPa, respectively. Thus, the cap pressures for the double-yield model are listed in Table 5.

A trial-and-error method was employed to determine the gob materials parameters by matching the stress–strain curve obtained by numerical modelling to that found by Eq. (1). For this purpose, a single-element sub-model with dimensions 1 m × 1 m × 1 m was generated. A constant velocity

Table 5 Cap pressures for the double-yield model

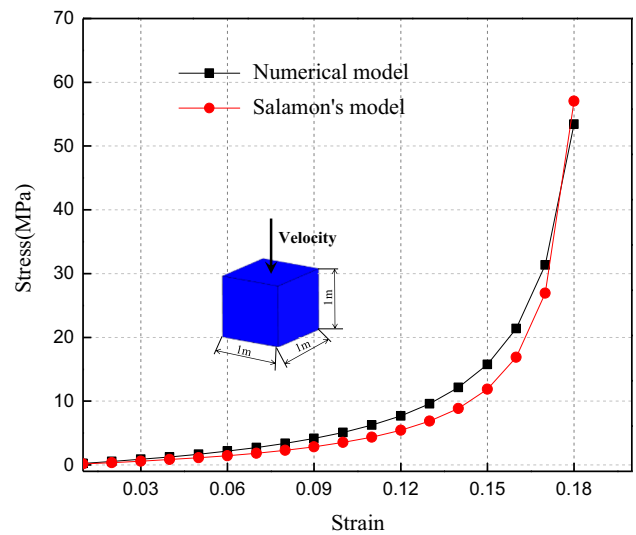| Strain	Stress (MPa)	Strain	Stress (MPa)
0.01	0.17	0.10	3.52
0.02	0.37	0.11	4.36
0.03	0.59	0.12	5.43
0.04	0.85	0.13	6.87
0.05	1.13	0.14	8.87
0.06	1.46	0.15	11.88
0.07	1.85	0.16	16.90
0.08	2.30	0.17	26.93
0.09	2.85	0.18	57.04

Fig. 9 Comparison of the stress–strain curve between the numerical model and Salamon's model

was applied to the top of the model in the negative z-direction to generate vertical loading on the model. The velocity magnitude was set at 10^{-5} m/s. The displacement of the four vertical planes of the model was restricted in the normal direction, and a zero vertical displacement condition was set at the base of the model. The input parameters were calibrated by an iterative change in the bulk modulus, shear modulus, the angle of dilation and the angle of friction of the gob materials. The stress–strain curve obtained from numerical model is plotted in Fig. 9, and a comparison with the stress–strain curve obtained by Salamon's model shows that they match very well. Table 6 presents the approved materials properties of the gob materials.

3.3.2 Verification of the Calibrated Double-Yield Model for Gob Modelling

To check the reliability of the gob model, the vertical stress of each zone inside the caved zone at simulation process

Table 6 Materials parameters for the double-yield model

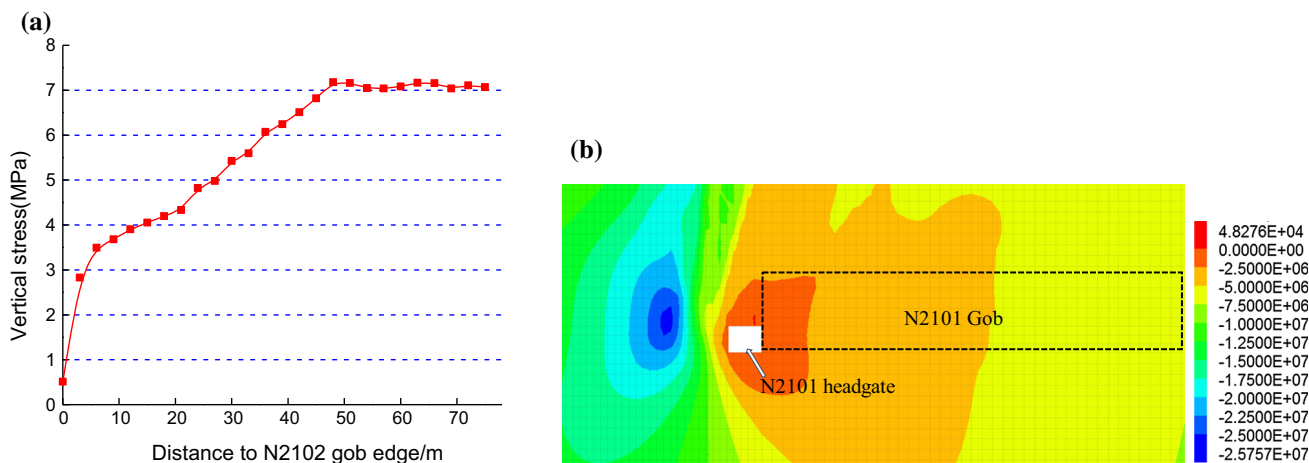| Parameters	Density (kg/m³)	Bulk modulus (GPa)	Shear modulus (GPa)	Friction (°)	Dilation (°)
Value	1000	8.87	6.73	22	7

(a)

(b)

Fig. 10 Vertical stress distribution of the N2101 gob after the modelling process (iii) i.e. the retreat of N2101 panel **a** simulated vertical stress changes in the N2101 gob, **b** simulated vertical stress distribution in the N2101 gob

(iii) was recorded and is plotted in Fig. 10. The vertical stress increases from 0.48 MPa at the gob edge to 7.16 MPa at a distance of about 50 m from the gob edge and then remains relatively constant. In other words, 95% of the original vertical stress (7.16/7.5 MPa) can be recovered at 17% of the panel overburden depth (48/298 m). Smart and Haley (1987) suggested that the reasonable estimate of cover stress distance should be 0.12 times overburden depth based on field measurement data. Based on an investigation and analysis of a large number of gateroad stability cases, Wilson (1981) suggested that the vertical stress increases from zero to the original stress at a distance of 0.2–0.3 times overburden depth. It can be seen that the stress distribution of the N2102 caved zone is in good agreement with other researchers' conclusions. Therefore, the calibrated parameters in Tables 5 and 6 can be used to model the gob materials.

3.4 Validation of the Global Model

To check the reliability of the global model, the measurement data in Fig. 6a were adopted to calibrate the input parameters in the simulation. Figure 11 shows a comparison between the measured and simulated convergences during the N2102 tailgate development period. The convergence curve obtained from numerical simulation matches field measurement data very well, thus confirming that the parameters used in the numerical models were reasonable and reliable.
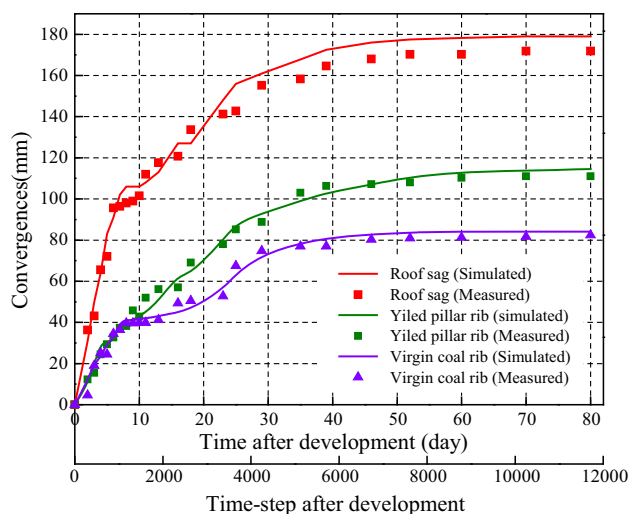

Fig. 11 Comparison of gateroad convergence predicted by numerical simulation and field measurement

4 Model Results and Yield Pillar Width Determination

4.1 Model Results

Figure 12 presents the model results. Taking Fig. 12a as an example, the shaded zone and blank zone represent the yielding state and elastic state of the elements surrounding the gateroad, respectively. The arrowed number represents the range of the yield zone. The two curves on the right and
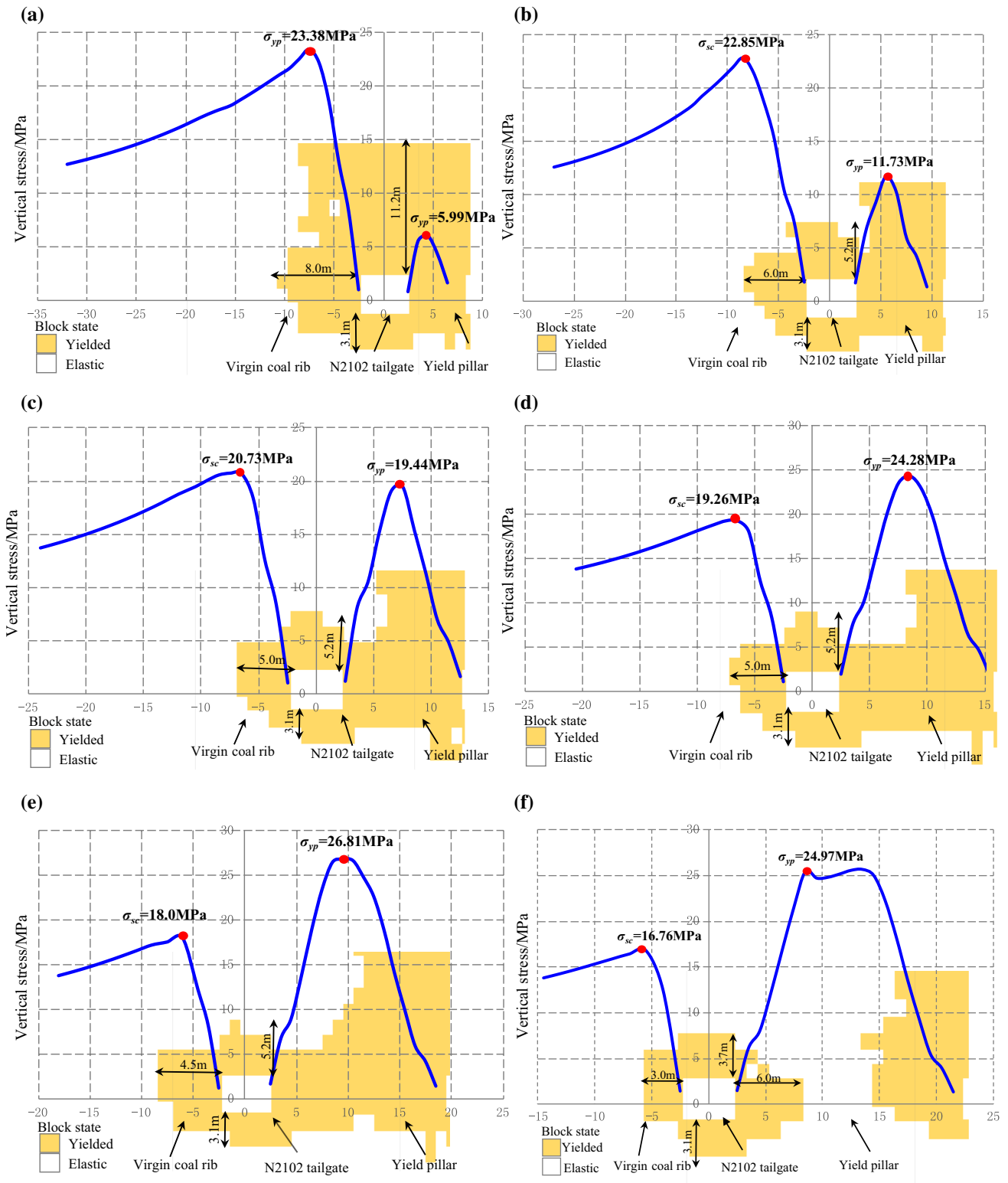
Fig. 12 Vertical stress and yield zone distributions around gateroads for different pillar widths. **a** Pillar width is 5 m, **b** pillar width is 8 m, **c** pillar width is 11 m, **d** pillar width is 14 m, **e** pillar width is 17 m, **f** pillar width is 20 m

left represent the vertical stress distribution in the yield pillar and virgin coal rib, respectively. The peak value of the vertical stresses in the yield pillar and virgin coal rib are marked as σ_{yp} and σ_{sc}, respectively. Notably, the data for both curves were obtained from the mid-height of the two ribs.

When the yield pillar width is 5 m (Fig. 12a), the yield pillar is crushed and cannot maintain gateroad stability. In this case, the ranges of yield zone in the gateroad roof, virgin coal rib and floor reach 11.2, 8.0 and 3.1 m, respectively. And σ_{yp} is merely 5.99 MPa and less than the virgin stress (7.5 MPa), while σ_{sc} maintains 23.38 MPa. When the yield pillar width varies from 8 to 11 m, as shown in Fig. 12b, c, the pillar is still in a yield state, but it is not crushed. The yield zone in the roof and virgin coal rib decreases to 5.2 and 5.0 m, respectively. Moreover, σ_{yp} increases gradually from 11.73 to 19.44 MPa, which is greater than the virgin stress but still less than σ_{sc}; in other words, the peak vertical stress is still located in the virgin coal rib. Conversely, when the yield pillar width ranges from 14 to 17 m, as shown in Fig. 12d, e, σ_{yp} increases sharply and becomes larger than σ_{sc}, indicating that the mining pressure is mainly undertaken by the yield pillar. When the yield pillar width equals 20 m (Fig. 12f), there is an intact core zone about 6 m wide in the yield pillar. The range of the yield zone surrounding the gateroad decreases significantly. And the distribution of vertical stress in the pillar changes from a "single peak" shape to a "double peak" shape, and σ_{yp} and σ_{sc} decrease slightly. As discussed above, it can be observed that the load-bearing capacity of the yield pillar is gradually improved with an increased yield pillar width, and the peak stress moves gradually from the virgin coal rib to the yield pillar rib. Therefore, we can improve the stress environment of the gateroad by adjusting the pillar width.

4.2 Yield Pillar Width Determination

4.2.1 Mechanical Principle of the Stress Changes in Two Ribs

Figure 12 shows that the final stress distribution characteristics in the yield pillar rib and virgin coal rib exhibit significant variation as the changes in yield pillar width. This is a result of stress redistribution induced by the mining and excavation activities. In actual mining engineering, due to the effect of mining stress induced by the gateroad excavation and panel retreat, the yield pillars are subjected to a complex loading and unloading process. Once the yield pillar is formed in the coal seam, mining-induced stress develops over it. The abutment pressure, previously undertaken by the coal masses, is transferred from the immediate roof to the yield pillar and virgin coal rib. When the pressure exceeds the ultimate strength of the coal, the edge of the coal is damaged with different degrees from shallow to deep, and then, the abutment pressure is transferred into the deep coal body. If the yield pillar width is large, the yield pillar has the sufficient bearing capacity to carry the mining stress (see Fig. 12e, f). Conversely, if the yield pillar width is small, its

bearing capacity is too weak and cannot undertake the mining stress; then, the stress was transferred to the deep part of the virgin coal rib (see Fig. 12a, b). An optimal pillar width should not only be benefit to increase coal recovery rate and achieve economic benefits, but also have a certain bearing capacity to withstand the mining stress and maintain gateroad integrity.

4.2.2 Determination of a Rational Yield Pillar Width

As discussed in the in situ measurement section, the original pillar width (17 m) and support pattern cannot maintain gateroad stability and production safety. The failure mechanism can be described as follows. During entry development, the gateroad excavation action leads to stress redistribution and the rock masses surrounding the gateroad are subjected to high stress. Owing to the surrounding rock structure and low coal strength, the roof and two ribs undergo severe deformation and gradually enter a yielding state. However, the mining stress is not shifted to the deep part of the virgin coal rib because of a higher bearing capacity of the yield pillar; that is, the gateroad is always located in a high-stress environment (see Fig. 12e). Combined with the effect of the front abutment stress caused by the panel N2102 retreat, large deformation and failure occurs in the gateroad.

The results of the simulations indicate that when yield pillar width equals 8 m, the peak stress jumps to the depth area of virgin coal rib and the pillar is subjected to a relatively low load. The rocks surrounding the gateroad are in a relatively low-stress environment and can maintain their stability with proper supports. Furthermore, the width of 8 m can significantly improve the coal recovery rate. Consequently, the rational yield pillar width can be estimated at 8 m.

4.3 Support Strategy

Based on successful experiences in many Chinese underground coal mines, the following support strategy is proposed:

1. Adopt bolts/cables with high strength and pretension in the roof strata. After influencing the peak pressure induced by the longwall mining, the top-slice coal of the N2103 tailgate is in the state of yielding (Fig. 12b), making it vulnerable to delamination, and thus leading to roof sagging. High pretension bolts can improve the integrity of the top coal, while high pretension anchor cables can be used to clamp the top coal to the stable rock strata.

2. Apply fully grouted bolts to the yield pillar rib. Because the pillar is in the state of yielding and most of the strain energy is fully released, it is necessary to adopt bolts

Fig. 13 Detailed support pattern in N2103 tailgate
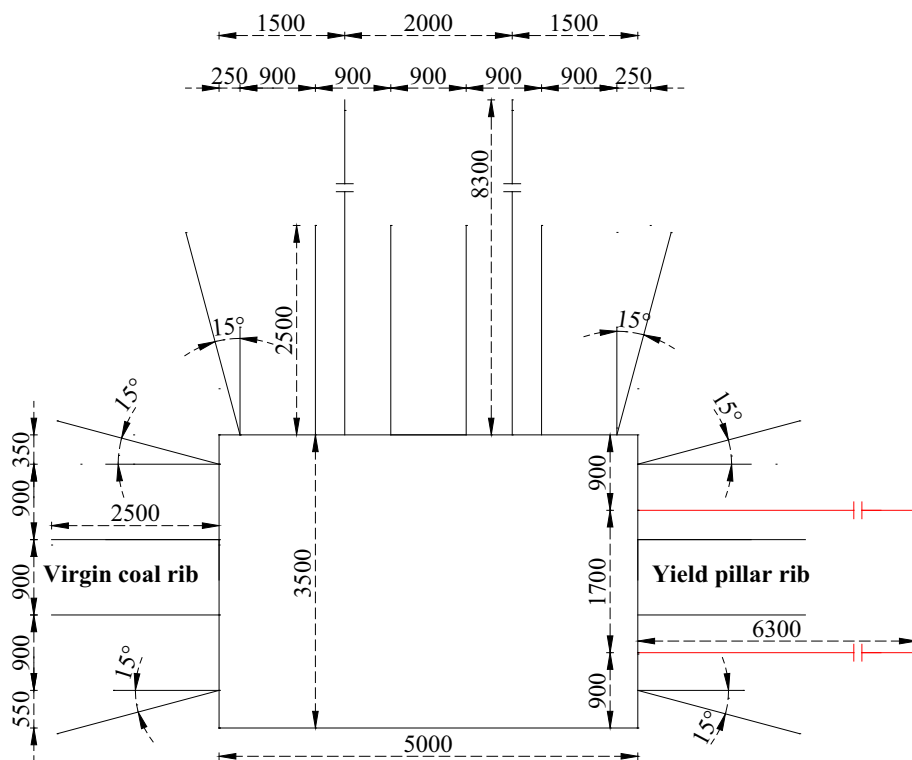
support to maintain the integrity of the yield pillar. In the yielded pillar rib, partially grouted bolts can easily lose their supporting function once their anchor point failure occurs (Shen 2013). To prevent this from occurring, fully grouted bolts should be used to ensure the effectiveness of the yield pillar support system.

3. Increase the support intensity of the virgin coal rib. The stability of the gateroad system is closely related to the virgin coal rib. When the yield pillar width is 8 m, the peak stress in virgin coal rib is 22.85 MPa. To ensure the stability of the virgin coal rib and release some strain energy, high-strength yielding bolts is necessary for the rib support.

4. Ensure reinforced support during N2103 panel retreat. The gateroad will experience high stress induced by the N2103 panel retreat, which will lead to severe deformation and failure in the gateroad. It is therefore necessary to employ anchor cables and hydraulic support to reinforce the yield pillar rib and roof in front of the working face (Wang et al. 2015).

5 Field Application and Implications

5.1 Field Application

Based on the support strategy mentioned above, a new gateroad support pattern was proposed and applied in the

N2103 tailgate. Figure 13 shows the details of bolt/cable arrangement in the gateroad cross section.

During the N2103 tailgate development period, high-strength bolts 20 mm in diameter and 2500 mm in length were used in the roof and yield pillar rib support. High-strength yielding bolts 20 mm in diameter and 2500 mm in length were used in the coal rib support. All bolts were installed with a spacing of 900 mm × 1000 mm. The bolts are made of high-strength steel bars with a yield strength of 400 MPa and an ultimate strength of 570 MPa. The bolts installed in the yield pillar rib are fully grouted using resin chemicals over the entire length. High-strength anchor cables 17.8 mm in diameter and 8300 mm in length were also used in the roof support. The cables were installed with a spacing of 2000 mm × 2000 mm. All bolts and anchor cables should be pretensioned with a pretension force of 70 and 200 KN, respectively.

During the N2103 panel retreat period, hydraulic prop support was used to reinforce the roof strata. Two props were set up in each row, and the rows were spaced at 1000 mm. The anchor cable 17.8 mm in diameter and 6300 mm in length was used in the yield pillar rib. The cables were installed with a spacing of 1700 mm × 2000 mm.

To validate the applicability of new pillar size and support pattern, the deformation of the surrounding rocks in the N2103 tailgate was traced during the gateroad development and panel retreat period, as illustrated in Fig. 14. The convergences in the roof, yield pillar rib and virgin coal rib after 30 days were
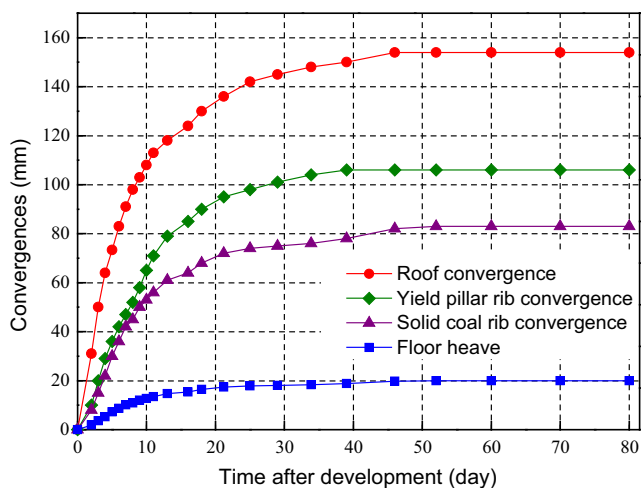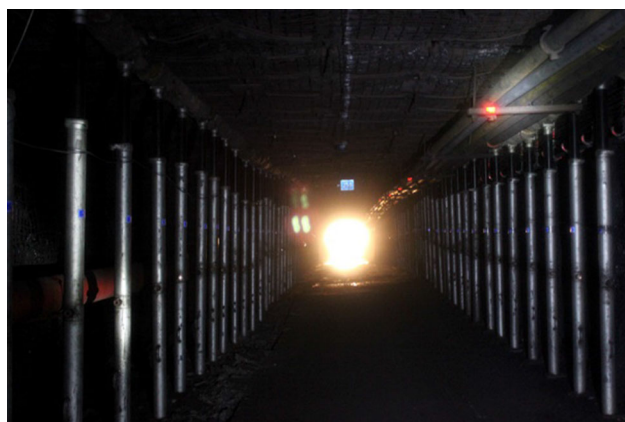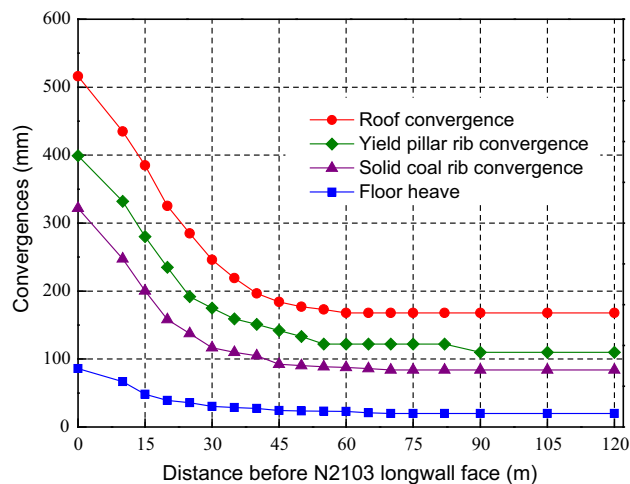
Fig. 14 Measured convergences in N2102 tailgate

Fig. 15 Gateroad profile before the longwall face

153, 107 and 84 mm, respectively. During the N2013 panel retreat period, the gateroad deformation increased considerably and the total convergences in the roof, yield pillar rib and virgin coal rib were 516, 398, 321 mm, respectively, which were 58, 68, 91% of the deformation that occurred when the previous pillar size and support pattern were used. The improvement in gateroad stability could also be visually observed on site. The photograph in Fig. 15 was taken at a gateroad location 60 m before the longwall face. The field measurement results confirmed the feasibility of current pillar size and support pattern.

5.2 Implications

The main function of the yield pillar is to protect the gateroads from the effects of excessive closure for a safe and stable gateroad condition. However, according to the literature review in the introduction section, it can be found that the approaches for the yield pillar design are miscellaneous and have some limitations, and there is no simple

and yet widely accepted yield pillar design principle. Therefore, it is important to propose a new approach and principle for yield pillar design.

Based on the performance of the yield pillar in the two case studies, we found that the yield pillar with a width of 17 m cannot maintain gateroad stability, while a yield pillar with a width of 8 m is effective in gateroad stability control. And, the numerical model results in Fig. 12 indicate that when the yield pillar width equals 17 m, the gateroad is located in a high-stress environment and the peak stress in the virgin coal rib and yield pillar rib reaches 26.8 and 18 MPa, respectively, which is nearly 2.4 and 3.6 times the initial ground stress, correspondingly. Conversely, when the yield pillar width equals 8 m, the peak stress jumps to the deep part of the virgin coal rib, the yield pillar is subjected to a low load and the rock masses surrounding the gateroad are in a relatively low-stress environment. As such, we can conclude that the majority of the abutment loads needs to be taken by the virgin coal rib, instead of the yield pillar, in order to have a well-functioned gateroad. This finding also indicates that the relationship between the peak vertical stresses in the two ribs could be a viable principle for yield pillar design.

Notably, different coal seams present great varieties in geological and production conditions, which lead to differences in optimal yield pillar size. However, the modelling procedure and design principle presented in this study are necessary in the design of yield pillars in other coal mines.

6 Conclusions

The aim of this case study carried out at Yuncheng city, Shanxi Province, China, was to investigate the gateroad stability in relation to the yield pillar width, based on a field

test, case studies and numerical modelling for back analysis. This study contains the following three original aspects:

1. A numerical modelling, using FLAC3D software, was developed for yield pillar design. As a new numerical approach, a double-yield model was used for modelling the gob materials, and its input parameters were meticulously calibrated based on a back-analysis procedure. Additionally, the global model was validated against the field monitoring data. This model procedure and calibrated method can provide a more reliable and realistic yield pillar design.

2. In order to have a well-functioned gateroad, the majority of the abutment loads needs to be taken by the virgin coal rib, instead of the yield pillar. This finding indicates that the relationship between the peak vertical stresses in the two ribs could be a viable principle for yield pillar design.

3. A new support strategy was proposed to adopt high strength and pretension bolts/cables in the roof strata, full length grouting in the yield pillar, increased intensity of support in the virgin coal rib and reinforced support during the current panel retreat. This strategy provides sufficient details to allow its application in other coal mines.

The test site is located at Yuncheng city, Shanxi Province, China. The average overburden depth of related panels is 298 m. The field investigations indicated that when the yield pillar width was 17 m, the total convergence of the roof, yield pillar rib and virgin coal rib were 882, 587 and 352 mm, respectively, and severe roof sagging and yield rib spalling occurred during the panel retreat. The model results revealed that when the yield pillar width equals 17 m, the peak stress in the yield pillar rib and virgin coal rib reaches 26.8 and 18 MPa, respectively; this high stress caused severe deformation in the rocks surrounding the N2012 tailgate. Conversely, when the yield pillar width is 8 m, the peak vertical stress is transferred to the deep part of the virgin coal rib and the pillar is subjected to a relatively low load. Consequently, the rational yield pillar width can be estimated at 8 m, and a new support strategy was proposed and applied in the field. Field tests indicated that the total convergences in the roof, yield pillar rib and virgin coal rib were 516, 398, 321 mm, respectively, which were 58, 68, 91% of the deformation that occurred when the previous pillar width and support pattern were used. The improvement in gateroad stability could also be visually observed on site.

References

Cai MF, He MC, Liu DY (2013) Rock mechanics and engineering, 2nd edn. Science Press, Beijing

Chen SJ, Wang HL, Wang HY, Guo WJ, Li XS (2016) Strip coal pillar design based on estimated surface subsidence in Eastern China. Rock Mech Rock Eng 49:3829–3838. doi:10.1007/s00603-016-0988-y

Cheng YM, Wang JA, Xie GX, Wei WB (2010) Three-dimensional analysis of coal barrier pillars in tailgate area adjacent to the fully mechanized top caving mining face. Int J Rock Mech Min Sci 47:1372–1383

Esterhuizen GS, Dolinar DR, Ellenberger JL (2011) Pillar strength in underground stone mines in the United States. Int J Rock Mech Min Sci 48:42–50. doi:10.1016/j.ijrmms.2010.06.003

Galvin JM, Hebblewhite BK, Salamon MDG (1999) UNSW coal pillar strength determinations for Australian and South African mining conditions. In: Proceedings of the 37th US rock mechanics symposium, Vali, Colorado, pp 63–71

Gao W (2014) Study on the width of the non-elastic zone in inclined coal pillar for strip mining. Int J Rock Mech Min Sci 72:304–310. doi:10.1016/j.ijrmms.2014.09.013

Itasca (2007) Fast lagrangian analysis of continua in 3 dimension, Version 3.1, User's guide. Minneapolis, USA

Jaiswal A, Shrivastva BK (2009) Numerical simulation of coal pillar strength. Int J Rock Mech Min Sci 46:779–788. doi:10.1016/j.ijrmms.2008.11.003

Jiang LS, Sainoki A, Mitri HS, Ma NJ, Liu HT, Hao Z (2016) Influence of fracture-induced weakening on coal mine gateroad stability. Int J Rock Mech Min Sci. doi:10.1016/j.ijrmms.2016.04.017

Li WF, Bai JB, Peng S, Wang XY, Xu Y (2014) Numerical modeling for yield pillar design: a case study. Rock Mech Rock Eng 48:305–318. doi:10.1007/s00603-013-0539-8

Li WF, Bai JB, Cheng J et al (2015) Determination of coal–rock interface strength by laboratory direct shear tests under constant normal load. Int J Rock Mech Min Sci 77:60–67

Medhurst TP, Brown ET (1998) A study of the mechanical behaviour of coal for pillar design. Int J Rock Mech Min Sci 35:1087–1105

Mohammad N, Reddish DJ, Stace LR (1997) The relation between in situ, and laboratory rock properties used in numerical modelling. In J Rock Mech Min Sci 34:289–297

Peng SS (2006) Longwall mining, 2nd edn. Peng SS publisher, Morgantown

Salamon MDG (1970) Stability, instability and design of pillar workings. Int J Rock MechMin Sci Geomech 7:613–631

Salamon M (1990) Mechanism of caving in longwall coal mining. Rock mechanics contributions and challenges: proceedings of the 31st US symposium on rock mechanics, Colorado, Golden, pp 161–168

Salamon MDG, Munro AH (1967) A study of strength of coal pillars. J S Afr Inst Min Metall 68:55–67

Salamon MDG, Ozbay MU, Madden BJ (1998) Life and design of bord-and-pillar workings affected by pillar scaling. J S Afr Inst Min Metall 98:135–145

Shabanimashcool M, Li CC (2013) A numerical study of stress changes in barrier pillars and a border area in a longwall coal mine. Int J Coal Geol 106:39–47

Shen BT (2013) Coal mine roadway stability in soft rock: a case study. Rock Mech Rock Eng 47:2225–2238. doi:10.1007/s00603-013-0528-y

Sheorey PR, Singh TN, Singh B (1982) Considerations for the stability of longwall chain pillars and adjacent roadway. In: Farmer IW (ed) Proceedings of the symposium on strata

mechanics, Newcastle-upon-Tyne. Elsevier, Amsterdam, pp 129–133

Smart BGD, Haley SM (1987) Further development of the roof strata tilt concept for pack design and the estimation of stress development in a caved waste. Min Sci Technol 5:121–130

Trueman R (1990) The application of a numerical model to longwall coal mine roadway design. Min Sci Technol 10:157–165

Wagner H (1974) Determination of the complete load-deformation characteristics of coal pillars. In: Proceedings of the third international congress on rock mechanics, Denver, pp 1076–1081

Wang M, Bai JB, Li WF, Wang XY, Cao SG (2015) Failure mechanism and control of deep gob-side entry. Arab J Geosci 8:9117–9131. doi:10.1007/s12517-015-1904-6

Wang SL, Hao SP, Chen Y, Bai JB, Wang XY, Xu Y (2016) Numerical investigation of coal pillar failure under simultaneous static and dynamic loading. Int J Rock Mech Min Sci 84:59–68. doi:10.1016/j.ijrmms.2016.01.017

Whittaker BN, Singh RN (1981) Stability of longwall mining gate in relation to rib pillar size. Int J Rock Mech Min Sci Geomech 18:331–334

Wilson AH (1981) Stress and stability in coal ribsides and pillars. In: Proceedings 1st conference on ground control in mining, West Virginia University, Morgantown, pp 1–12

Yavuz H (2004) An estimation method for cover pressure re-establishment distance and pressure distribution in the goaf of longwall coal mines. Int J Rock Mech Min Sci 41:193–205. doi:10.1016/s1365-1609(03)00082-0

Yu B, Zhang ZY, Kuang TJ, Liu JR (2016) Stress changes and deformation monitoring of longwall coal pillars located in weak ground. Rock Mech Rock Eng 49:3293–3305

Zhang GC, He FL (2016) Asymmetric failure and control measures of large cross-section entry roof with strong mining disturbance and fully-mechanized caving mining. Chin J Rock Mech Eng 35:806–818. doi:10.13722/j.cnki.jrme.2015.0917

Zhang K, Zhang GM, Hou RB, Wu Y, Zhou HQ (2014) Stress evolution in roadway rock bolts during mining in a fully mechanized longwall face, and an evaluation of rock bolt support design. Rock Mech Rock Eng 48:333–344. doi:10.1007/s00603-014-0546-4